

- 125 ⁴⁷ *Qufu Normal University, Qufu 273165, People's Republic of China*
 126 ⁴⁸ *Shandong Normal University, Jinan 250014, People's Republic of China*
 127 ⁴⁹ *Shandong University, Jinan 250100, People's Republic of China*
 128 ⁵⁰ *Shanghai Jiao Tong University, Shanghai 200240, People's Republic of China*
 129 ⁵¹ *Shanxi Normal University, Linfen 041004, People's Republic of China*
 130 ⁵² *Shanxi University, Taiyuan 030006, People's Republic of China*
 131 ⁵³ *Sichuan University, Chengdu 610064, People's Republic of China*
 132 ⁵⁴ *Soochow University, Suzhou 215006, People's Republic of China*
 133 ⁵⁵ *South China Normal University, Guangzhou 510006, People's Republic of China*
 134 ⁵⁶ *Southeast University, Nanjing 211100, People's Republic of China*
 135 ⁵⁷ *State Key Laboratory of Particle Detection and Electronics, Beijing 100049, Hefei 230026, People's Republic of China*
 136 ⁵⁸ *Sun Yat-Sen University, Guangzhou 510275, People's Republic of China*
 137 ⁵⁹ *Suranaree University of Technology, University Avenue 111, Nakhon Ratchasima 30000, Thailand*
 138 ⁶⁰ *Tsinghua University, Beijing 100084, People's Republic of China*
 139 ⁶¹ *Turkish Accelerator Center Particle Factory Group, (A)Istinye University, 34010, Istanbul, Turkey; (B)Near East University, Nicosia, North Cyprus, 99138, Mersin 10, Turkey*
 140 ⁶² *University of Chinese Academy of Sciences, Beijing 100049, People's Republic of China*
 141 ⁶³ *University of Groningen, NL-9747 AA Groningen, The Netherlands*
 142 ⁶⁴ *University of Hawaii, Honolulu, Hawaii 96822, USA*
 143 ⁶⁵ *University of Jinan, Jinan 250022, People's Republic of China*
 144 ⁶⁶ *University of Manchester, Oxford Road, Manchester, M13 9PL, United Kingdom*
 145 ⁶⁷ *University of Muenster, Wilhelm-Klemm-Strasse 9, 48149 Muenster, Germany*
 146 ⁶⁸ *University of Oxford, Keble Road, Oxford OX13RH, United Kingdom*
 147 ⁶⁹ *University of Science and Technology Liaoning, Anshan 114051, People's Republic of China*
 148 ⁷⁰ *University of Science and Technology of China, Hefei 230026, People's Republic of China*
 149 ⁷¹ *University of South China, Hengyang 421001, People's Republic of China*
 150 ⁷² *University of the Punjab, Lahore-54590, Pakistan*
 151 ⁷³ *University of Turin and INFN, (A)University of Turin, I-10125, Turin, Italy; (B)University of Eastern Piedmont, I-15121, Alessandria, Italy; (C)INFN, I-10125, Turin, Italy*
 152 ⁷⁴ *Uppsala University, Box 516, SE-75120 Uppsala, Sweden*
 153 ⁷⁵ *Wuhan University, Wuhan 430072, People's Republic of China*
 154 ⁷⁶ *Xinyang Normal University, Xinyang 464000, People's Republic of China*
 155 ⁷⁷ *Yantai University, Yantai 264005, People's Republic of China*
 156 ⁷⁸ *Yunnan University, Kunming 650500, People's Republic of China*
 157 ⁷⁹ *Zhejiang University, Hangzhou 310027, People's Republic of China*
 158 ⁸⁰ *Zhengzhou University, Zhengzhou 450001, People's Republic of China*
 159
 160
 161 ^a *Also at the Moscow Institute of Physics and Technology, Moscow 141700, Russia*
 162 ^b *Also at the Novosibirsk State University, Novosibirsk, 630090, Russia*
 163 ^c *Also at the NRC "Kurchatov Institute", PNPI, 188300, Gatchina, Russia*
 164 ^d *Also at Goethe University Frankfurt, 60323 Frankfurt am Main, Germany*
 165 ^e *Also at Key Laboratory for Particle Physics, Astrophysics and Cosmology, Ministry of Education; Shanghai Key Laboratory for Particle Physics and Cosmology; Institute of Nuclear and Particle Physics, Shanghai 200240, People's Republic of China*
 166 ^f *Also at Key Laboratory of Nuclear Physics and Ion-beam Application (MOE) and Institute of Modern Physics, Fudan University, Shanghai 200443, People's Republic of China*
 167 ^g *Also at State Key Laboratory of Nuclear Physics and Technology, Peking University, Beijing 100871, People's Republic of China*
 168 ^h *Also at School of Physics and Electronics, Hunan University, Changsha 410082, China*
 169 ⁱ *Also at Guangdong Provincial Key Laboratory of Nuclear Science, Institute of Quantum Matter, South China Normal University, Guangzhou 510006, China*
 170 ^j *Also at Frontiers Science Center for Rare Isotopes, Lanzhou University, Lanzhou 730000, People's Republic of China*
 171 ^k *Also at Lanzhou Center for Theoretical Physics, Lanzhou University, Lanzhou 730000, People's Republic of China*
 172 ^l *Also at the Department of Mathematical Sciences, IBA, Karachi 75270, Pakistan*

M($\ell^+ \ell^-$) AT EACH CENTER-OF-MASS ENERGY

178 Figure 1 shows the $M(\ell^+ \ell^-)$ at each c.m. energy ($\sqrt{s} = 4.61 - 4.95$ GeV)

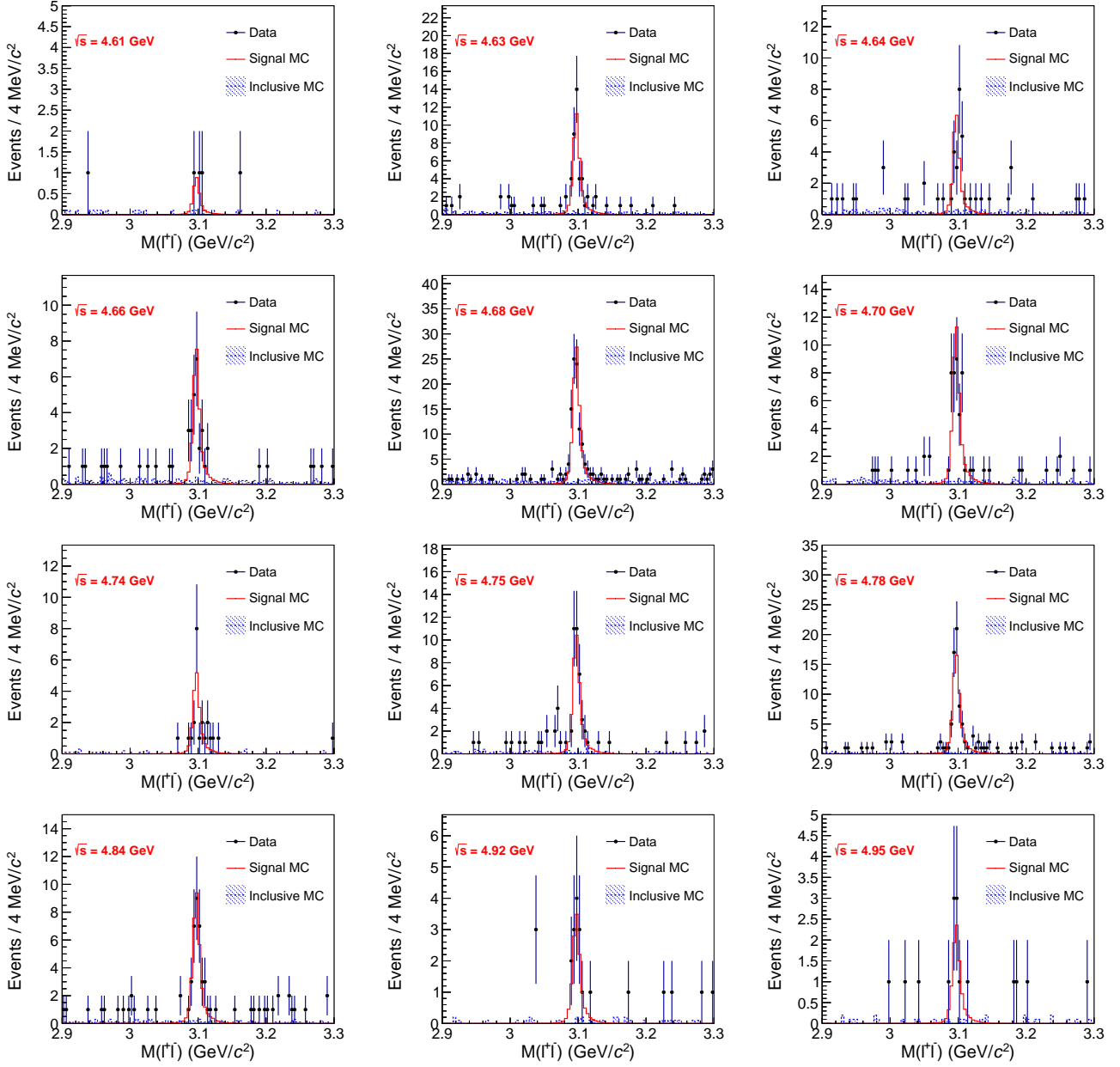


Fig. 1. The $M(\ell^+ \ell^-)$ distribution at each c.m. energy. Dots with error bars are data, the red histograms are signal MC and the blue shaded histograms stand for the background from the inclusive MC samples.

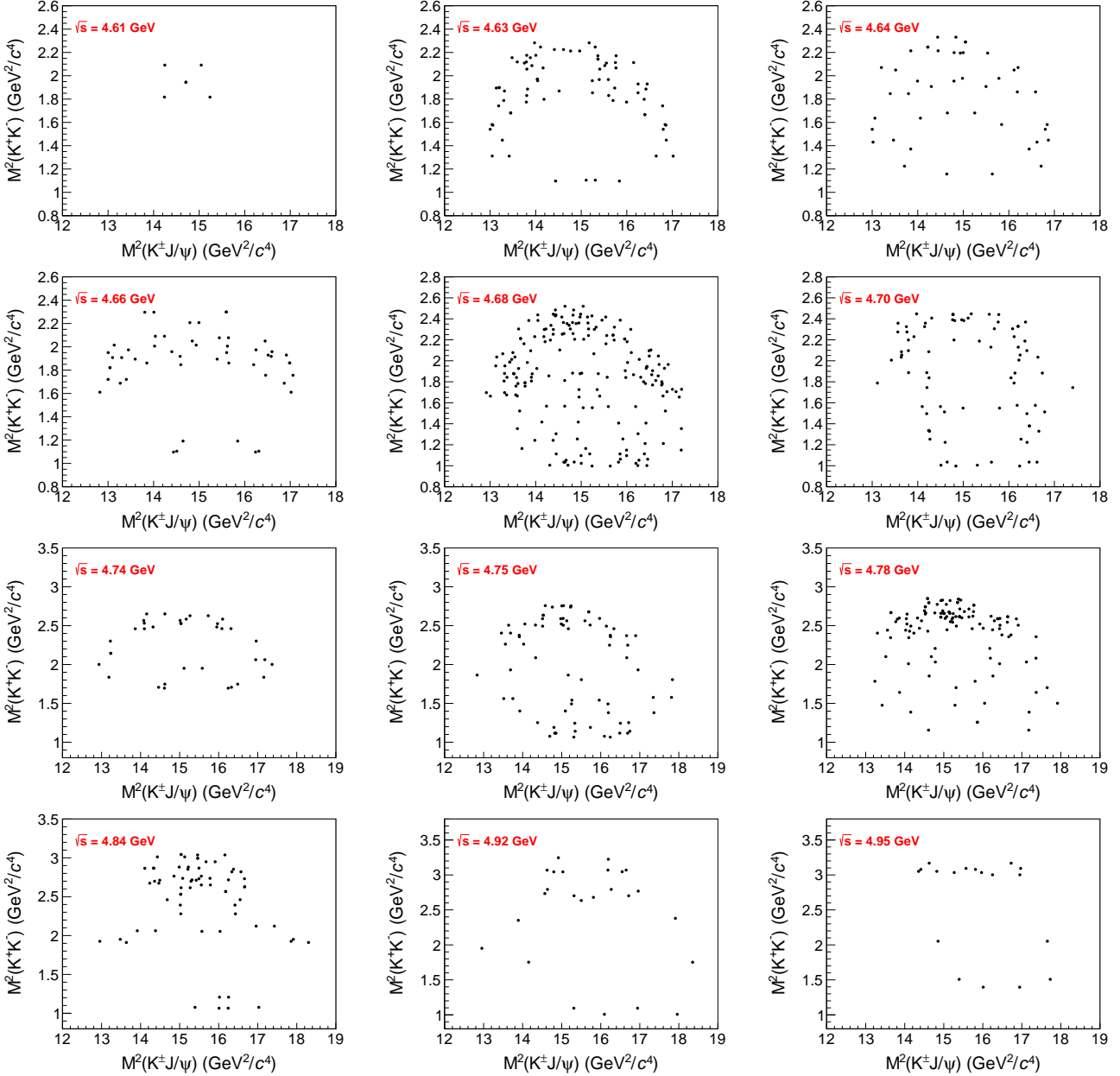


Fig. 2. The Dalitz plots of the data samples at each c.m. energy.

180

CROSS SECTIONS

181 The c.m. energies (\sqrt{s}), integrated luminosities (\mathcal{L}), numbers of events in the signal region (N^{obs}) and in the
 182 sideband regions (N^{side}), signal yields (N^{sig}), event selection efficiencies (ϵ), ISR correction factors ($(1 + \delta)$), vacuum
 183 polarization factors ($|1 + \Pi|^2$), Born cross sections (σ^{Born}), and Born cross section ratios of $e^+e^- \rightarrow K_S^0 K_S^0 J/\psi$ to
 184 $e^+e^- \rightarrow K^+ K^- J/\psi$ ($\frac{\sigma^{\text{Born}}(K_S^0 K_S^0 J/\psi)}{\sigma^{\text{Born}}(K^+ K^- J/\psi)}$) are shown in Table 1.

185 In the maximum likelihood fit to the dressed cross sections of $e^+e^- \rightarrow K^+ K^- J/\psi$, assuming the obtained signal
 186 events obey Poisson ($N^{\text{sig}} \leq 10$) or asymmetric Gaussian ($N^{\text{sig}} > 10$). The Poisson is defined as

$$P_{\text{Poisson}} = (N^{\text{fit}} + f \cdot N^{\text{side}})^{N^{\text{obs}}} \cdot \frac{e^{-(N^{\text{fit}} + f \cdot N^{\text{side}})}}{N^{\text{obs}}!}, \quad (1)$$

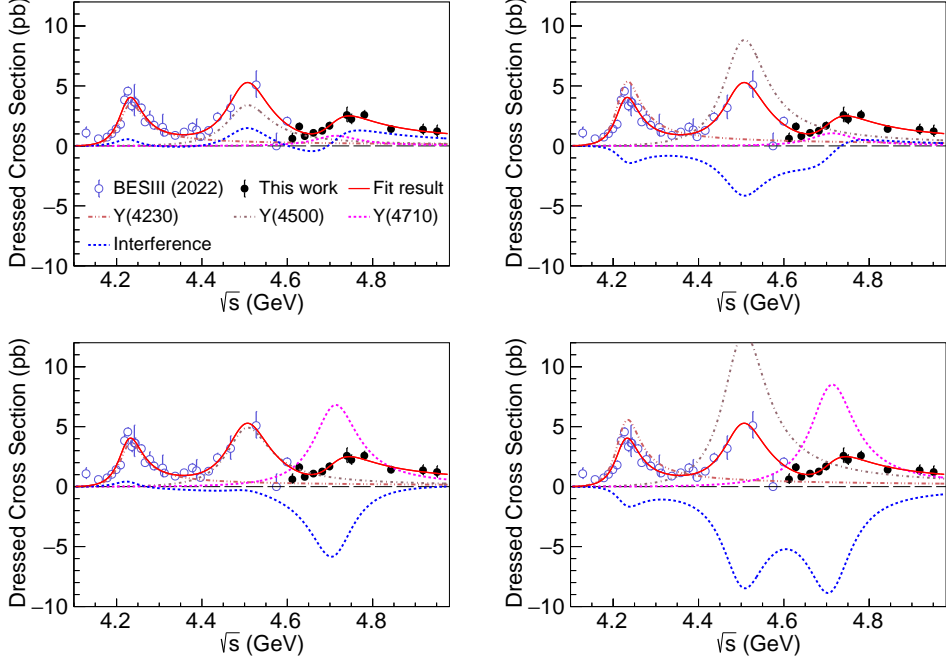


Fig. 3. Four solutions of the fits to the dressed cross sections of $e^+e^- \rightarrow K^+K^-J/\psi$ with the coherent sum of three Breit-Wigner functions (solid curve). The dash (dash-dot-dot or dash-dot) curve shows the contribution from the three structures $Y(4710)$ ($Y(4230)$ or $Y(4500)$). The solid dots with error bars are the cross sections from this study, and the dash dots with error bars are the cross sections from Ref. [1]. The error bars are statistical uncertainty only.

Tab. 3. The systematic uncertainties in the measurement of resonance parameters, including that due to the c.m. energy (\sqrt{s}), the parameterization of the fit function (Fitting), the c.m. energy spread (ES), and the uncommon (σ_1^{Dress}) and common (σ_2^{Dress}) systematic uncertainties from the cross section measurement. The symbol “–” represents the uncertainty, which can be neglected.

Parameter	\sqrt{s}	Fitting	ES	σ_1^{Dress}	σ_2^{Dress}	Sum
M_3 (MeV/ c^2)	0.80	20.91	0.11	3.03	–	21.1
Γ_3 (MeV)	–	29.67	0.01	1.09	–	29.7
	–	0.09	–	–	0.01	0.09
$(\Gamma_{ee}\mathcal{B})_3$ (eV)	–	0.01	–	–	0.01	0.01
	–	0.26	–	0.03	0.04	0.26
	–	0.06	–	0.03	0.05	0.08
	–	0.40	–	0.08	–	0.41
ϕ_3 (rad)	–	0.69	–	0.08	–	0.69
	–	0.42	0.01	0.02	–	0.42
	–	0.70	–	0.02	–	0.70

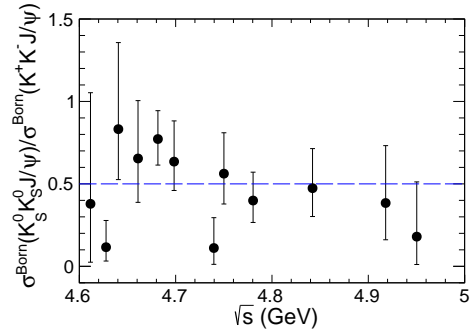


Fig. 4. Ratio of Born cross section $\sigma^{\text{Born}}(e^+ e^- \rightarrow K_S^0 K_S^0 J/\psi)$ to $\sigma^{\text{Born}}(e^+ e^- \rightarrow K^+ K^- J/\psi)$, where the error bars are statistical only.

202

SYSTEMATIC UNCERTAINTIES ON THE Z_{cs} MEASUREMENT

203 Systematic uncertainties for the Born cross sections of Z_{cs} states include the detection efficiencies, vacuum polarization
 204 and ISR factor, which are estimated in the cross section measurement of $e^+e^- \rightarrow K^+K^-J/\psi$. These uncertainties
 205 are multiplicative.

Tab. 4. Systematic uncertainties on the Z_{cs} Born cross sections. The first five uncertainties are additive systematic uncertainties on the yields of Z_{cs} while the last two uncertainties are multiplicative.

Source	Systematic uncertainty on <i>yields</i> or efficiencies
Detector resolution	0.1
Efficiency curves	Negligible
Signal model	0.2
Backgrounds	0.1
f states	0.3
Z_{cs} resonance parameters	See the main texts
Detection efficiency	15%

206 In addition, we take into account the systematic uncertainties from the detector resolution, efficiency curves,
 207 signal models of Z_{cs} , backgrounds and f states, Z_{cs} resonance parameters, which are summarized in Table 4. The
 208 difference of detector resolution between data and MC is estimated to be 3.2 MeV/ c^2 by studying the control sample
 209 of $e^+e^- \rightarrow K^+D^{*0}D_s^{*-}$. We smear the resolution function and redo the $M_{\max}(K^\pm J/\psi)$ fit and the change is taken
 210 as the systematic uncertainty. Through the similar procedure to estimate systematic uncertainties, we vary the
 211 efficiency curves within $\pm 1\sigma$ uncertainties, change the signal model under different J^P assumptions, vary the kernel
 212 width parameter of the background shapes and add shapes of f state at $\sqrt{s} > 4.70$ GeV. We also generate signal MC
 213 samples for each signal model, and we take the largest difference between the resultant efficiencies and the nominal
 214 efficiencies as the systematic uncertainty. We vary the resonance parameters within $\pm 1\sigma$ regions and take the largest
 215 changes of the yields as the uncertainties.

216 These additive systematic uncertainties on the fitted yields are then converted into Born cross sections. Then the
 217 the root of quadratic sum of converted uncertainties and multiplicative uncertainties, which will be discussed later, is
 218 assigned as the σ of a Gaussian function. Then the Gaussian function will be used to convolve with the distributions
 219 of the nominal $-\ln L$ values.

220 Multiplicative uncertainties are related to the detection efficiencies, vacuum polarization and ISR factor, which part
 221 of which has been estimated in the measurement of the line shape. Except for the uncertainty of MC model which is
 222 irrelevant to detection efficiencies of Z_{cs} , all uncertainties in the measurement of line shape will be considered in the
 223 convolution of systematic uncertainties. Different spin-parity assumptions will affect the angular distribution of final
 224 states thus affect the detection efficiencies. We take the largest relative change among all energies to the nominal
 225 uncertainty in different spin-parity assumptions, 15.0%, as the systematic uncertainty.

226 The convolved $-\ln L$ distributions are shown in red curves in Figs. 5 and 6, which are used to determine the upper
 227 limits at the 90% confidence level. The upper limits are shown in Table 5.

Tab. 5. The detection efficiencies ϵ , and upper limits $\sigma^{\text{Born}}(e^+e^- \rightarrow K^-Z_{cs}^+ + c.c.) \cdot \mathcal{B}(Z_{cs}^+ \rightarrow K^+J/\psi)$ of Born cross sections for Z_{cs} states at the 90% confidence level, where the systematic uncertainties are incorporated. The VP and ISR factors are taken from Table 1.

\sqrt{s} (GeV)	$\epsilon(Z_{cs}(3985))$	$\epsilon(Z_{cs}(4000))$	$\sigma^{\text{Born}} \cdot \mathcal{B}[Z_{cs}(3985)]^{\text{UL}}$ (pb)	$\sigma^{\text{Born}} \cdot \mathcal{B}[Z_{cs}(4000)]^{\text{UL}}$ (pb)
4.63	0.408	0.409	0.2	0.9
4.64	0.402	0.399	0.2	0.7
4.66	0.404	0.396	0.2	0.7
4.68	0.415	0.414	0.1	0.8
4.70	0.428	0.429	0.2	3.3
4.74	0.456	0.449	0.6	1.9
4.75	0.444	0.445	0.3	1.5
4.78	0.426	0.428	0.3	0.8
4.84	0.397	0.401	0.3	1.4
4.92	0.376	0.375	0.6	1.3

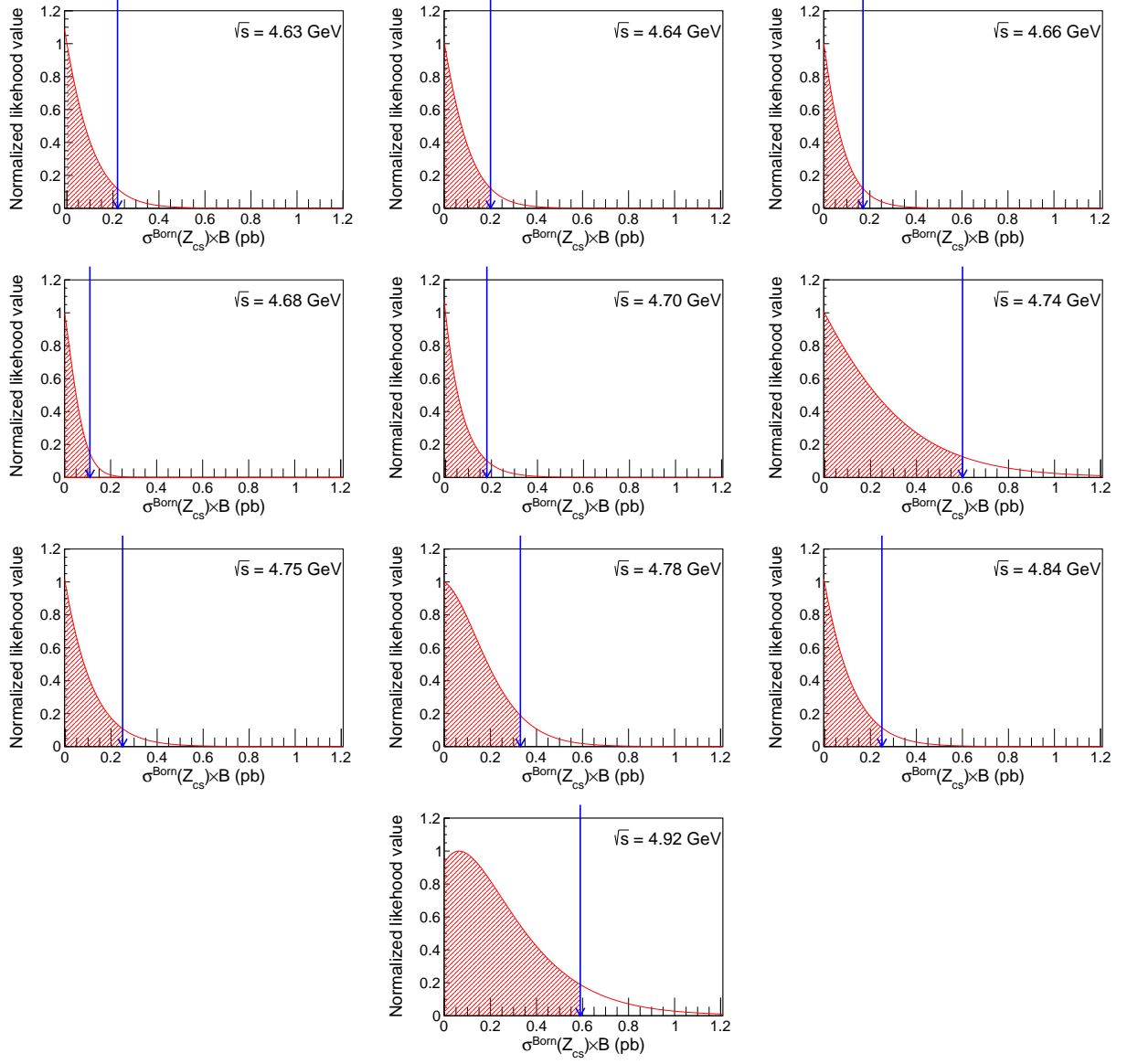


Fig. 5. The scans for the upper limits of Born cross sections of $e^+e^- \rightarrow K^- Z_{cs}(3985)^+ + c.c.$. The blue arrows indicate the upper limits at the 90% confidence level by integrating the red regions consisting of smeared likelihood values with systematic uncertainties considered.

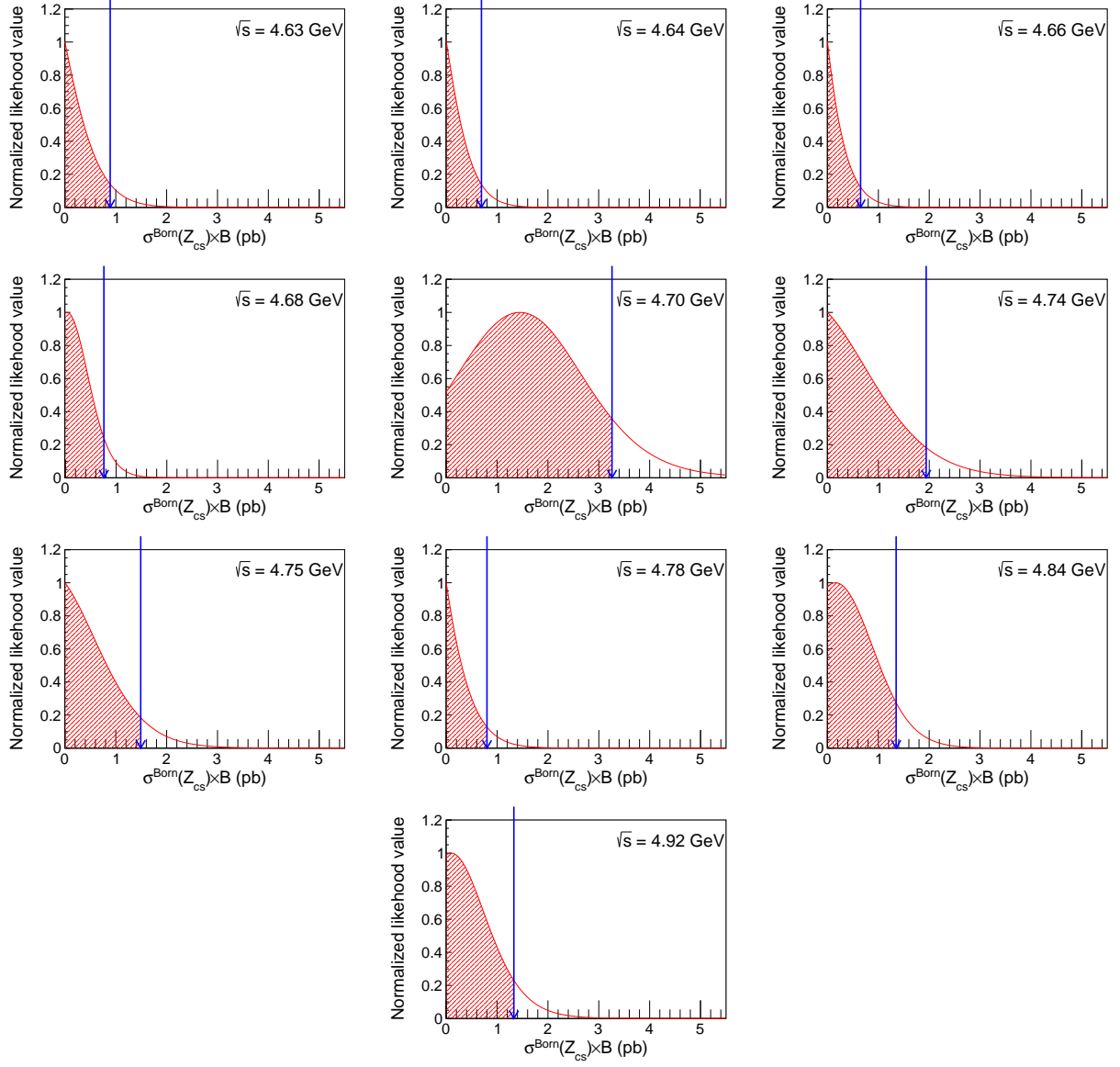


Fig. 6. The scans for the upper limits of Born cross sections of $e^+e^- \rightarrow K^- Z_{\text{cs}}(4000)^+ + c.c.$. The blue arrows indicate the upper limits at the 90% confidence level by integrating the red regions consisting of smeared likelihood values with systematic uncertainties considered.

PARTIAL WAVE ANALYSIS

229 Partial wave analysis (PWA) using helicity formalism is performed on each c.m. energy to study the intermediate
 230 states. However, no significant Z_{cs} signal is detected because of the limited statistics. The $f_0(0^{++})$ and $f_2(2^{++})$
 231 components can be not well distinguished either. The PWA results with different $f_{0,2}$ combinations are used to
 232 generate alternative signal MC samples to do efficiency uncertainty study for $e^+e^- \rightarrow K^+K^-J/\psi$ cross section
 233 measurement. Figures 7 and 8 show the comparison of distributions between data and one of the PWA results at four
 234 c.m. energies with higher statistics ($\sqrt{s} = 4.68, 4.70, 4.78, 4.84$ GeV). For the data sets with $\sqrt{s} \leq 4.70$ GeV, the PWA
 235 results are based on the $f_0(980) + f_0(1500)$ assumption. For the data sets with $\sqrt{s} > 4.70$ GeV, the PWA results are
 236 based on a single $f_0(x)$ with mass and width free in the fit.

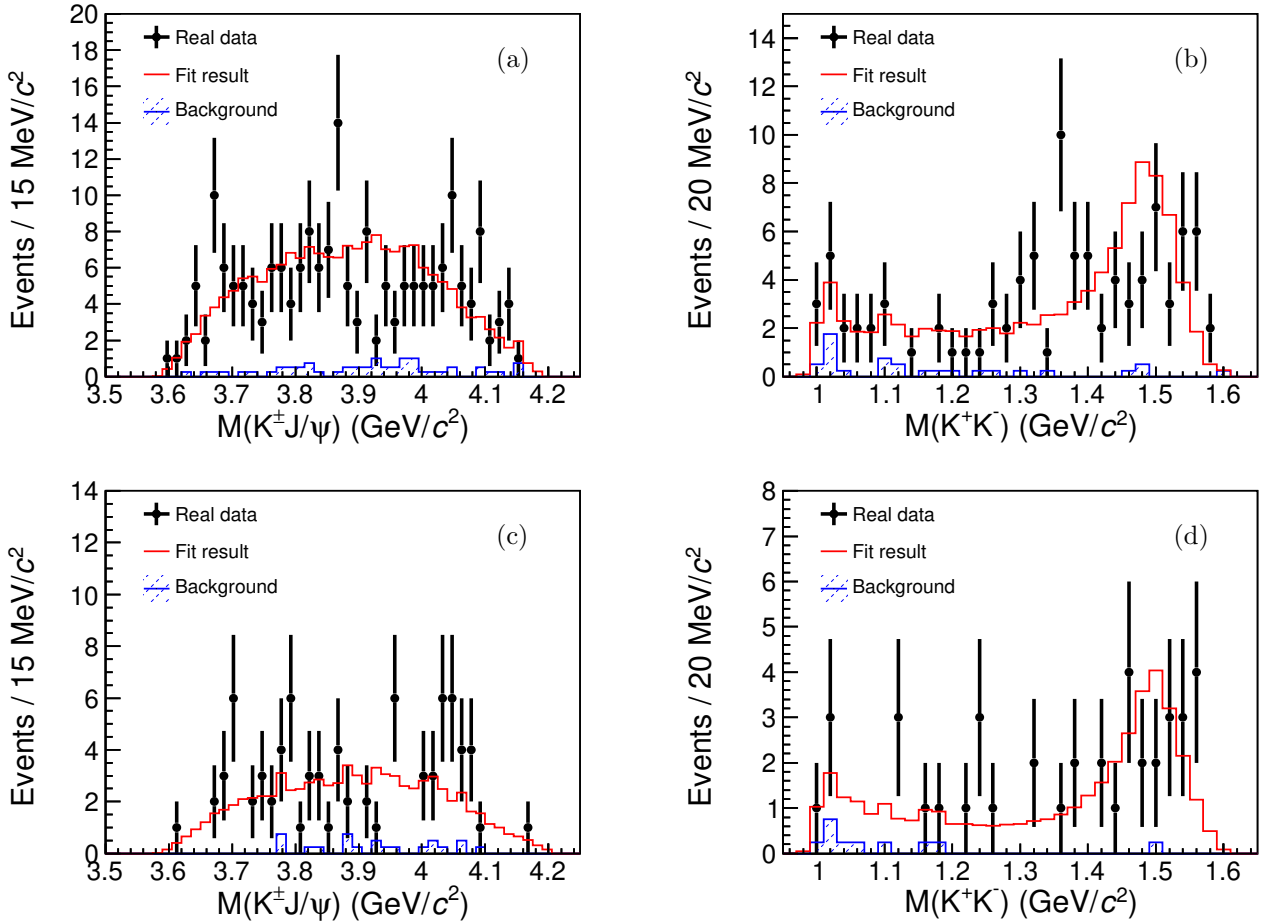


Fig. 7. The comparisons of $M(K^\pm J/\psi)$ and $M(K^+K^-)$ between real data and the PWA result. The black dots with error bars are real data, the red line is the sum of the fit result and background from J/ψ sideband. The PWA results at (a, b) $\sqrt{s} = 4.68$ GeV and (c, d) $\sqrt{s} = 4.70$ GeV are based on the $f_0(980) + f_0(1500)$ assumption.

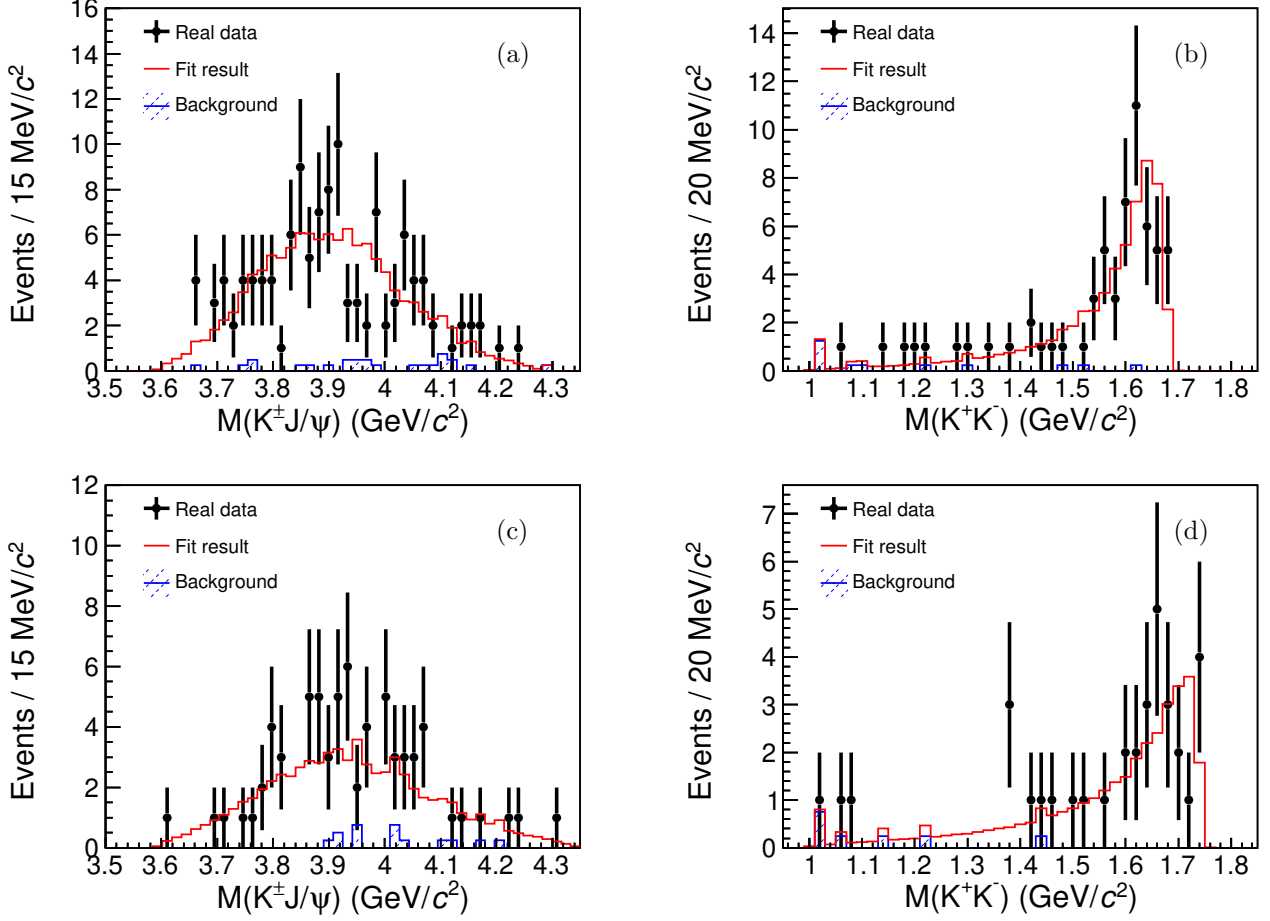


Fig. 8. The comparisons of $M(K^\pm J/\psi)$ and $M(K^+ K^-)$ between real data and the PWA result. The black dots with error bars are real data, the red line is the sum of the fit result and background from J/ψ sideband. The PWA results at (a, b) $\sqrt{s} = 4.78 \text{ GeV}$ and (c, d) $\sqrt{s} = 4.84 \text{ GeV}$ are based on a single $f_0(x)$ with mass and width free in the fit.

²³⁷ [1] M. Ablikim *et al.* (BESIII Collaboration), Chin. Phys. C **46**, 111002 (2022), arXiv:2204.07800 [hep-ex].
²³⁸ [2] M. Ablikim *et al.* (BESIII Collaboration), Phys. Rev. D **107**, 092005 (2023), arXiv:2211.08561 [hep-ex].